Supplementary Information

Cap-Sweat: A capillary microfluidic platform for digitized sweat sampling and time-resolved biomarker analysis

Pezhman Jalali[1,2], Amir Sanati Nezhad[1,3*]

[1] BioMEMS and Bioinspired Microfluidics Laboratory, Department of Biomedical Engineering, University of Calgary, Calgary, AB T2N 1N4, Canada
[2] Biomedical Engineering Program, University of Calgary, Calgary, AB T2N 1N4, Canada
[3] Department of Mechanical and Manufacturing Engineering, University of Calgary, Calgary, AB T2N 1N4, Canada

[*]Corresponding author:
Amir Sanati Nezhad
amir.sanatinezhad@ucalgary.ca

Table of Contents

Note S1. Cap-Sweat geometry and governing physics

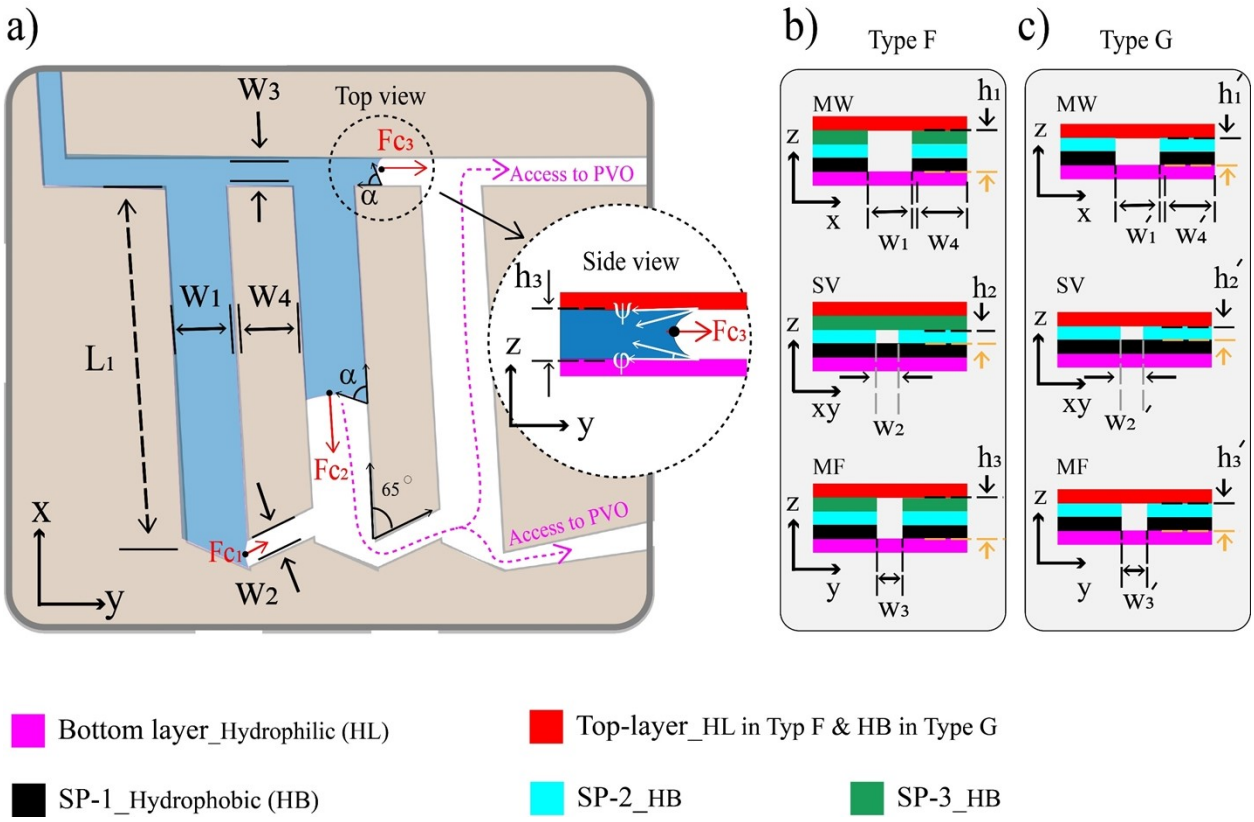

Figure S1. Cap-Sweat geometry and governing physics. a) Top view of the capillary element showing the geometric parameters of each section and the resulting capillary pressure distribution governing sequential filling. **b)** Cross-sectional view of the Cap-Sweat Type-F architecture highlighting hydrophilic and hydrophobic surface interfaces. **c)** Cross-sectional view of the Cap-Sweat Type-G architecture highlighting hydrophilic and hydrophobic surface interfaces.

Note S1.1 Geometry and layout parameters

Figure S1.a Schematic representation of the Cap-Sweat device geometry, indicating the defined width, length, and height of key capillary elements, including the stop valve (SV), main-flow channel (MF), and microchambers (CHs). The associated geometric parameters are provided in Table S1 (Geometry section). Figures S1b and S1c present the layer configuration and the hydrophilic/hydrophobic properties of the Cap-Sweat Type F and Type G designs separately. Figure S2b highlights Type F, in which the top and bottom layers are hydrophilic, while the SV is hydrophobic on all four sides to prevent liquid from crossing the valve. Figure S1c illustrates Type G, where Spacer-3 (SP-3) is removed and the top layer is modified to be hydrophobic; the SV remains fully hydrophobic in this configuration. Accordingly, both designs are operational, generating sufficient capillary driving force to transport sweat through the MF channel and into the CHs while maintaining reliable flow control at the SV when required.

Table S1. Geometric, wetting, capillary pressure, hydraulic resistance, and calculated flow rate parameters for Cap-Sweat Type F and Type G devices.

NO.	PARAMETER	TYPE F	TYPE G
	Geometry and layout parameters	**mm**	
1	Device dimensions (width × length)	32 mm × 50 mm	32 mm × 50 mm
2	Device thickness	0.6 mm	0.4 mm
3	CH width (W_1, W_1')	1 mm	1 mm
4	CH length (L_1, L_1')	6 mm	6 mm
5	Distance between adjacent CHs (W_4, W_4')	1 mm	1 mm
6	CH height (H_1, H_1')	0.3 mm	0.2 mm
7	MF width (W_3, W_3')	0.5mm	0.5 mm
8	MF height (H_3, H_3')	0.3mm	0.2 mm
9	SV width (W_2, W_2')	0.25 mm	0.25 mm
10	SV height (H_2, H_2')	0.6 mm	0.6 mm
11	Inlet height	0.5 mm	0.3 mm
12	Inlet coverage area	120 mm^2	120 mm^2
	Sweat Wetting properties	º	
13	Contact angle with MF & CH bottom layer (Φ)	12.3º	12.3º
14	Contact angle with MF & CH top layer (Ψ)	12.3°	12.3°
15	Contact angle with MF & CH vertical walls (α)	85°	83.4°
16	Contact angle with SV surfaces (all sides)	85 °	85°
17	Sweat surface tension	42.7 mN/m	42.7 mN/m
	Capillary Pressure	Pa	
18	ΔP_{SV}, Capillary pressure at SV boundary	-104	-104
19	ΔP_{CH}, Capillary pressure in CH	-286	-235
20	ΔP_{MF} , Capillary pressure at MF	-293	-242
	Hydraulic resistance	$\times 10^9$ Pa·s·m^{-3}	
21	Rh-SV, hydraulic resistance	64.1	64.1
22	Rh-CH, hydraulic resistance	0.54	1.7
23	Rh-MF, hydraulic resistance	1.42	4.0
	Flow rate	mL/min	mL/min
24	Q-SV, SV flow rate	0.1	0.1
25	Q-CH, CH flow rate	31.3	8.29
26	Q-MF, MF flow rate	12.38	3.63

SV, stop valve; MF, main-flow channel; CH, microchamber

Note S1.2 Stop valve positive capillary pressure

ΔP-SV represents the capillary pressure at the SV and air-conduit boundary, as illustrated in Figure S1a. These pressures were calculated using the Young–Laplace equation (Eq. S1):

$$\Delta P = -\gamma\left[\frac{\cos\theta_t + \cos\theta_b}{h} + \frac{\cos\theta_l + \cos\theta_r}{w}\right] \qquad \textit{Eq. S1}$$

where h and w denote channel height and width, respectively; γ is liquid surface tension; and θ_t, θ_b, θ_l, and θ_r represent static contact angles at the top, bottom, left, and right surfaces.

As shown in Table S1, ΔP-SV is negative, indicating that the capillary pressure barrier at the SV is insufficient to prevent forward liquid propagation under static conditions.. This arises because the contact angle of sweat on the SV surface—although intended to be fully hydrophobic—is approximately 85°, which is insufficient to generate a positive capillary pressure barrier. Consequently, sweat could potentially pass through the SV and reach the subsequent CH, leading to system failure.

As discussed in Section 3, this limitation is addressed by implementing a series CC configuration, which minimizes the duration during which the SV is exposed to the passive vent outlet (PVO) after sweat reaches its boundary. In this design, sweat cannot pass through the SV once the subsequent CH is filled. The flow rate into the next CH is approximately 300 times greater than the flow rate through the SV (see Table S1, flow-rate section), due to the higher capillary pressure and lower hydraulic resistance of the CH pathway. This difference in flow rates ensures that the downstream CH fills rapidly, effectively locking the preceding SV and enabling reliable system operation in the series CC configuration.

The hydraulic resistance was calculated using Eq. S2, and the corresponding flow rates were determined from the pressure–flow relationship in Eq. S3.

$$Rh = \frac{12\mu l}{wh^3\left[1 - \frac{192h}{\pi^5 w} + \sum_{n=1}^{\infty}\frac{1}{n^5}\tanh\frac{n\pi w}{2h}\right]} \qquad \textit{Eq. S2}$$

$$Q = \Delta P / Rh \qquad \textit{Eq. S3}$$

For all calculations, the channel length was assumed to be 1 mm.

Note S1.3 Successful Sequential CH Filling in the Presence of Capillary Pressure

Cap-Sweat is designed for time-resolved chrono-sampling of sweat. To ensure accurate temporal resolution, newly secreted sweat must sequentially fill each CH before advancing to the next CH. A potential concern arises from the positive value of ΔP_{MF} observed in both the F and G designs (Table S1), which suggests that sweat could propagate through the MF channel and enter the subsequent CH before the previous one is filled. The consistency of Cap-Sweat in chrono-sampling is primarily governed by geometric flow programming, which defines the hydraulic resistance (R_h) distribution between the CH and MF pathways. Therefore, the potential flow rate (Q), calculated using Eq. S3 under the assumption of sufficient liquid supply at the inlet, is approximately three times higher in the CH than in the MF channel.

If the sweat secretion rate were to exceed the potential Q_CH, simultaneous filling of the CH and MF could theoretically occur. However, typical human sweat rates (< 30 μL/min) are substantially lower than the calculated Q_CH values (~31 mL/min for Type F and ~8 mL/min for Type G). Therefore, under physiological conditions, the capillary–hydraulic programming dictated by the device geometry governs flow distribution, ensuring preferential CH filling and preserving temporal resolution. This behavior is experimentally demonstrated in Video S1 (Type F), where an inlet flow rate of 18 μL/min was applied, showing successful sequential filling of the CHs. Although a syringe pump was used to regulate the volumetric input, the system operated entirely under capillary-driven conditions. The inlet remained open to ambient air, and the pump did not impose an external pressure head; it merely supplied fluid at a controlled rate. Thus, flow direction, distribution, and sequential CH filling were governed exclusively by the intrinsic capillary pressure and the geometrically defined hydraulic resistance network.

Notably, for Type G, the calculated Q_CH (~8 mL/min) remains substantially higher than physiological sweat secretion rates (< 30 μL/min). Consequently, Type F—despite generating a higher capillary driving force—is not strictly necessary for effective sweat transport under normal operating conditions.

Accordingly, unlike prior chrono-sampling platforms fabricated from hydrophobic materials—which inhibit spontaneous capillary transport and therefore rely on sweat gland pressure to drive flow—the present design avoids pressure-driven operation. In those systems, limited wettability combined with capillary burst valves required elevated inlet pressures to enforce sequential filling. In contrast, the current design is intrinsically capillary-active and eliminates burst valves, achieving reliable sequential CH filling solely through capillary forces and geometrically programmed hydraulic resistance.

Note S2. Evaluation of Fiber-Assisted Inlet Designs for Minimizing Priming Volume

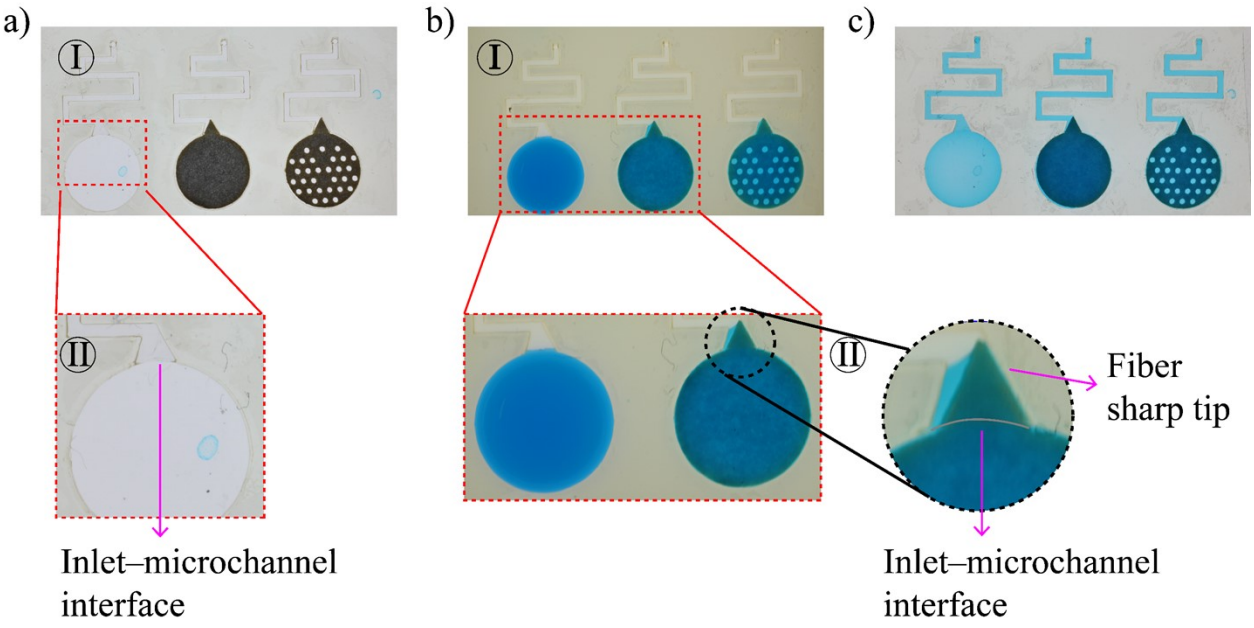

Figure S2. a (I) Schematic of the three-inlet design incorporating inlets without fiber, with fiber, and with patterned fiber. (II) Enlarged view of the inlet–microchannel interface where priming occurs. Sample was introduced at 20 µL/min using a syringe pump. **b** (I) Fully hydrophobic configuration showing complete confinement of the sample within the inlet, indicating the inability of hydrophobic channels to autonomously initiate flow. (II) Sharp fiber tip delivering absorbed sample across the inlet–microchannel interface. **c** Sample transport in hydrophilic channels, where capillary forces drive fluid entry and propagation without external pressure.

Here we designed an in-vitro test using the three-inlet platform shown in Figure S2a-I. The device consists of three inlets arranged from left to right: without fiber, with fiber, and with patterned fiber. The input sample was injected using a syringe pump at a constant flow rate of 20 µL/min. In this study, we evaluated the priming volume, defined as the amount of sample that accumulates inside the inlet before it can pass the inlet–microchannel interface (Figure S2a-II). The priming volume depends on the presence or absence of fiber inside the inlet and on the hydrophobic or hydrophilic nature of the microchannel.

Accordingly, three-inlet platforms were fabricated using fully hydrophobic, semi-hydrophobic (Type G), hydrophilic (Type F-1), and very hydrophilic (Type F-2) materials. In the fully hydrophobic structure, both the top and bottom layers are hydrophobic. In Type G, the top layer is hydrophilic while the bottom layer is hydrophobic, providing capillary force for sample transport. In Type F-1 and Type F-2, both layers are hydrophilic, with contact angles of 15° and

8°, respectively. Figure S2b-I shows the result for the fully hydrophobic structure, where the sample does not enter the microchannel even when the inlet is fully loaded. This demonstrates a limitation of conventional sweat-collection microfluidic devices that rely solely on hydrophobic structures and therefore depend entirely on sweat-gland pressure to drive fluid into the channel. Figure 2c illustrates the advantage of capillary-driven channels, where the sample advances through the microchannel even in the absence of gland pressure.

The in-vitro results are summarized in Table S2, showing that the presence of fiber substantially reduces the priming volume, particularly in Type G (from ~80 μL to ~13.5 μL). This reduction is achieved through the capillary absorption of the fiber—especially important for Type G with its hydrophobic inlet—and through the sharp fiber tip (Figure S2b-II). The sharp fiber tip effectively eliminates the burst-valve effect at the inlet–microchannel interface by delivering the absorbed sample directly into the microchannel, removing the need for large sample accumulation before release. Once the sample reaches this point, capillary action in the microchannel continues to pull the liquid forward. The results also show that the fiber saturation time decreases when the fiber is patterned with holes, which is the configuration implemented in the final Cap-Sweat design.

Table S2. Priming volume (μL) required for initiating flow in microchannels with different inlet configurations and material wettability.

Material Type	Without Fiber	With Fiber	Patterned Fiber
Type G (semi-hydrophilic)	80	16	13.5
Type F-1 (hydrophilic, 15°)	32	16	13.3
Type F-2 (very hydrophilic, 8°)	27	14.3	13

Note S3. In-vitro experiment of chrono-sampling

In an in-vitro experiment, a controlled mixture of purple and yellow dyes was introduced into the Cap-Drop-Sweat using two independent syringe pumps, each capable of regulating the flow rate of its respective dye. The flow rates were modulated dynamically to mimic the varying biomarker concentrations over time, as shown in Fig. S3.

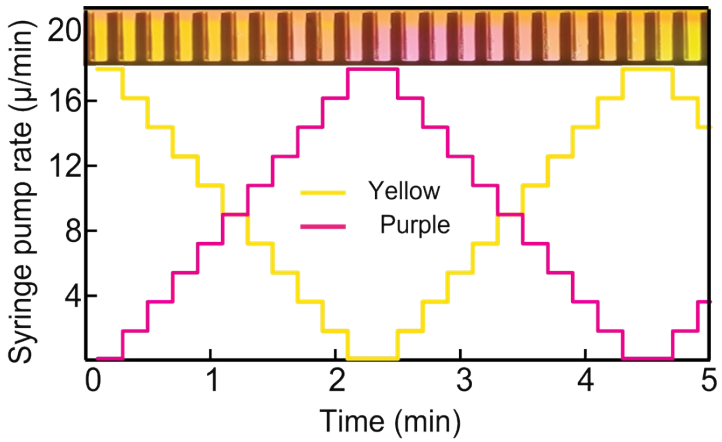

Fig. S3. Controlled injection rate of purple and yellow dye mixtures through the inlet via syringe pumps causes the formation of the same pattern in microchambers (CHs).

Note S4. Sweat secretion rate

Systematic sweat sampling reveals important temporal changes in sweat composition, offering valuable insights for tracking athletic performance, hydration levels, and disease biomarkers. In this study, the wearable Cap-Drop-Sweat device, equipped with 24 CHs each holding 3 μL (in type F), was used to monitor dynamic changes in sweat rate over time (Fig. S4).

Fig. S4. Calculation of sweat rate using the wearable Cap -Drop-Sweat system containing 24 CHs.

Figure S5 present sweat rate data across 24 CHs during a 20-min exercise period, extracted from Figure S4. A clear early peak in sweat rate was observed during the first 3–5 min, followed by a fluctuating but generally lower secretion rate in the remaining period. This initial spike mirrors previously reported physiological responses to thermoregulatory demand: Baker et al.[1] documented elevated sweat rates in the early stages of heat exposure, while Taylor and Machado-Moreira[2] described sympathetic-driven eccrine activation that quickly plateaus due to thermoneutral feedback. This observation supports the hypothesis that sweat dynamics are governed by a two-phase physiological model: (i) a sympathetic surge that rapidly activates eccrine glands, and (ii) a regulatory feedback phase where sweat rate and composition modulate based on thermal and metabolic cues.

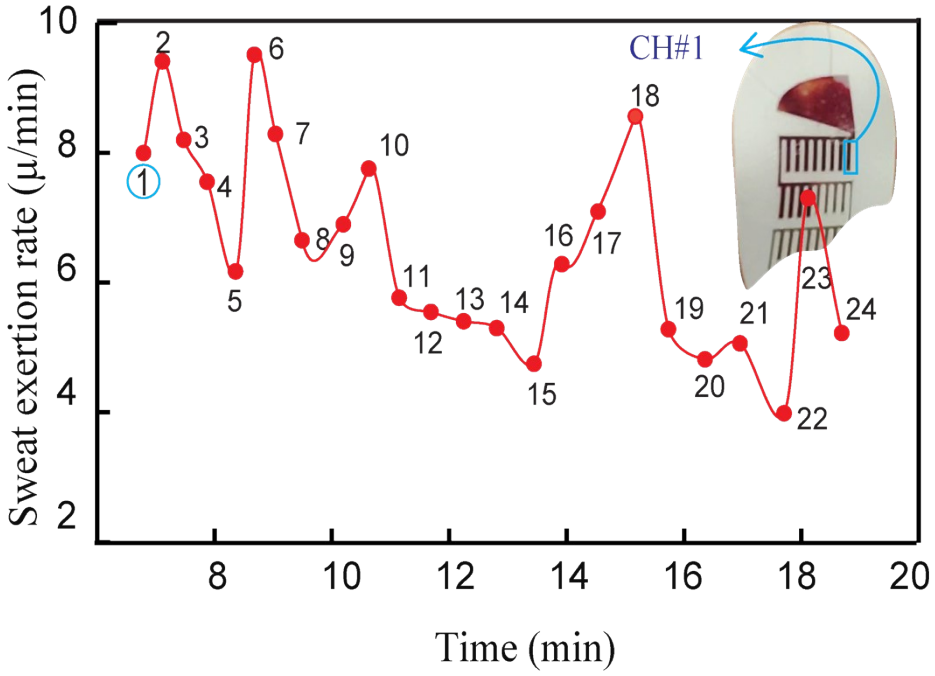

Fig. S5. Corresponding sweat excretion rates measured across 24 CHs profiles from three subjects, enabling high-resolution quantification of dynamic sweat secretion kinetics

Note S5. The calibration curve of the ELISA test

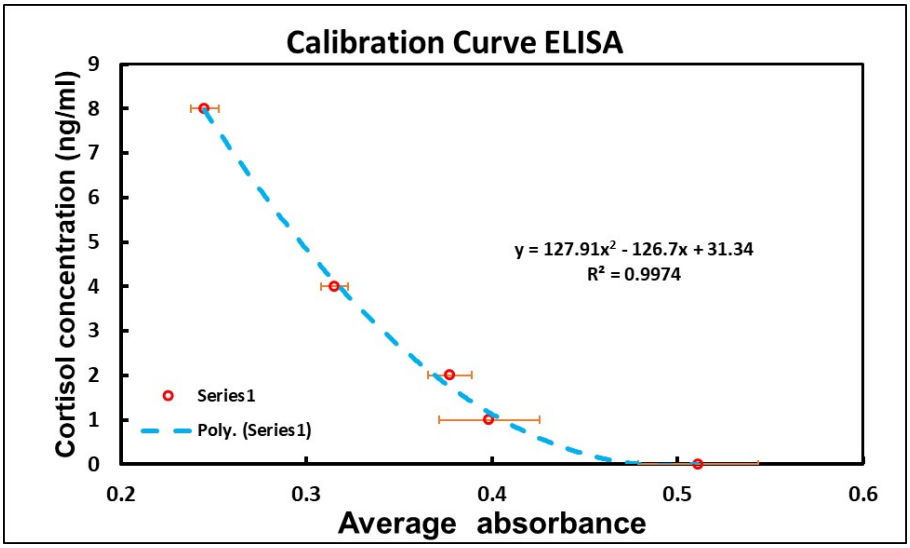

Fig. S6. The calibration curve used to measure cortisol concentration using the ELISA assay.

Note S6. Cap-Sweat volumetric capacity, operational window, and adaptability

The Cap-Sweat device used in this study contains 18 CHs, each with a defined volume of approximately 3 μL (in type F), yielding a total CHs capacity of ~54 μL. Prior to delivery into the microfluidic network, the inlet fiber requires approximately 13–15 μL of sweat to become fully saturated (Figure S1), after which sweat is transferred into the device. This inlet saturation volume can be reduced by decreasing the inlet dimensions. As a result, the first CH fills after approximately ~18 μL of sweat secretion.

Full operation of the device requires filling the channel network connecting all CHs, which requires an additional ~30 μL of sweat. Taken together, the complete 18-CH configuration reaches full capacity at approximately 99–103 μL of sweat. Under the sweat-rate conditions examined in this study, this corresponds to a total system operation time of approximately 15 minutes, representing the maximum temporal window over which full chrono-sampling is achieved.

Importantly, the minimum functional volume is substantially lower. Because each CH is physically isolated and fills strictly in sequence, effective chrono-sampling begins immediately once the first CH is filled (~18 μL). At this point, the device is fully operational and capable of delivering time-segmented samples, albeit over a shorter temporal window. As sweat secretion continues, additional CHs fill sequentially, extending the sampling duration.

The modularity of Cap-Sweat enables straightforward adaptation for longer-duration measurements if required in future studies. Each inlet–channel–CH unit functions as an independent capillary module that can be reconfigured by adjusting inlet dimensions, material combinations, CH volumes, or channel lengths, or by cascading additional CH arrays. Accordingly, the platform is not inherently constrained to short-duration monitoring; rather, the present configuration intentionally demonstrates its ability to resolve rapid biomarker dynamics during high-intensity physiological tasks, where short-term, high-temporal-resolution data are most informative.

References

1. L. B. Baker and A. S. Wolfe, *European Journal of Applied Physiology*, 2020, **120**, 719-752.
2. N. A. Taylor and C. A. Machado-Moreira, *Extreme Physiology & Medicine*, 2013, **2**, 1-30.